Computer-Aided Detection of Brain Metastases using a Three-Dimensional Template-Based Matching Algorithm

Úrsula Pérez-Ramírez, Estanislao Arana, and David Moratal, *Senior Member,* IEEE

***Abstract*— The purpose of this work was to develop an algorithm for detecting brain metastases in magnetic resonance imaging (MRI), emphasizing the reduction of false positives. Firstly, three-dimensional templates were cross-correlated with the brain volume. Afterwards, each lesion candidate was segmented in the three orthogonal views as a previous step to remove elongated structures such as blood vessels. In a database containing 19 patients and 62 brain metastases, detection algorithm showed a sensitivity of 93.55%. After applying the method for false positive reduction, encouraging results were obtained: false positive rate per slice decreased from 0.64 to 0.15 and only one metastasis was removed, leading to a sensitivity of 91.94%.**

I. Introduction

Brain metastases (BM) occur in approximately one quarter of adult cancer patients, being lung tumors the most common source. The cognitive and motor signs caused by BM decrease life quality and can even threaten patients' life without proper treatment in time. Therefore, it is of vital importance to detect BM in their initial stage. Diagnosis is carried out by means of magnetic resonance imaging (MRI) and computed tomography (CT) imaging [1].

Computer-aided diagnosis (CAD) plays a key role in assisting radiologists in a more accurate diagnosis. It allows to reduce human errors, minimizing user subjectivity and workload. Furthermore, its ability to reveal the number of lesions, their location and their size is of great clinical importance for planning the best treatment [1].

There are different methodologies for brain metastases detection. Most of them employ spherical tumor appearance models and a three-dimensional (3D) cross-correlation [2-5] to identify likely positions of BM, making use of brain atlas or preprocessing to remove false positives (FP) [2-4]. Other authors decided to reduce the number of detected blood vessels by applying a contrast-enhanced 3D black-blood pulse sequence in which dynamic blood was selectively suppressed while stationary tumor contrast remained [5]. Other choice is unsupervised change detection based on symmetry that searches for the most dissimilar region between the left and the right hemisphere in each axial slice, but it is only suitable for medium and large BM [6, 7]. Current work presents a 3D template-based matching algorithm and a segmentation-based method applied to MR brain images with the main objective of identifying a high percentage of BM while introducing a reasonably small number of FP.

The authors thank the financial support of the Spanish Ministerio de Economía y Competitividad (MINECO) and FEDER funds under Grant TEC2012-33778.

Úrsula Pérez-Ramírez and David Moratal are with the Center for Biomaterials and Tissue Engineering, Universitat Politècnica de València, Cami de Vera, s/n, 46022, Valencia, Spain (corresponding author e-mail: dmoratal@eln.upv.es).

Estanislao Arana is with the Radiology Department, Fundación Instituto Valenciano de Oncología, Valencia, Spain.

II. Materials and Methods

A. Patient database and data acquisition

Nineteen patients (11 men, 8 women, aged 65±23 years old) were scanned using a 1.5 T MR scanner, with an in-plane resolution of 1 mm and a slice thickness and separation between slices of 1.3 mm. These T1-weighted contrast-enhanced images were obtained using a spoiled gradient echo pulse sequence (SPGR) and a 256×256 matrix size. This dataset contained a total of 62 metastases, with a major diameter from 2.5 to 44.1 mm (median = 7.75 mm).

B. Template-based matching detection

Brain metastases are spheroid-like structures which are well-circumscribed and brighter than surrounding anatomical tissue on postcontrast MR brain scans. Taking into account these morphological features, 3D varying radii templates based on [2,8] were created using MATLAB 8.1 (The MathWorks, Inc., Natick, MA, USA). These templates were modified to be ellipsoidal, hollow and symmetric with respect to their center. In contrast, the authors created spherical and compact templates with three combinations, depending on the intersection between the image and the center of the sphere (above, below or exact). Zero padding allowed to find well-demarcated borders through the inclusion of a uniform number of black voxels surrounding the border of the template.

For templates creation, anisotropy of the voxels was taken into account through the ratio between slice thickness and in-plane resolution, *ratio*. Other parameters were *subvoxels*, the number of neighbor pixels considered to establish the intensity of a pixel, and *znum*, the multiplication of *ratio* by *subvoxels*. Then, the outer radii of the ellipsoid, a_1, b_1 and c_1 were defined in millimeters and converted to pixels. All the templates had a small inner hole, whose radii a_2 and b_2 were the quarter part of the corresponding outer radii, and c_2 a smaller pixel than c_1. The maximum of the three outer radii, *max_radius,* contributed to a parameter related to zero padding, N, calculated following (1):

$$N = (2 \cdot max\_radius + 1) \cdot subvoxels. \quad (1)$$

Then, two N×N×N matrices were initialized with zeros, and ones were placed at the coordinates *XCoord*, *YCoord* and

ZCoord which belonged to the outer and inner ellipsoid, respectively, as defined in (2):

$$\frac{XCoord^2}{a^2}+\frac{YCoord^2}{b^2}+\frac{ZCoord^2}{c^2}\leq 1. \quad (2)$$

Subsequently, the second matrix was subtracted from the first matrix and a hollow ellipsoid was obtained, resulting in *pretemplate* matrix. Zero padding was applied to this matrix in *x*, *y* and *z* [2,8], increasing the number of slices and leading to *pretemplate_pad* of size *xx*×*yy*×*zz*.

Reaching the end, a *xx*/*subvoxels*×*yy*/*subvoxels*×*zz*/*znum template* matrix was initialized to zero. Then, *subvoxels* rows, *subvoxels* columns and *znum* slices were caught from *pretemplate_pad* and mean intensity was placed by rows from left to right in each of the slices of *template*. That was, firstly the first row and the first column of each slice, then the first row and the second column of each slice and so on until the last row and the last column of the last slice were reached. Finally, all the black slices were removed.

Three templates were employed, with following dimensions: 6×5×4 mm^3, 7×8×9 mm^3 and 14×12×12 mm^3, and 5 *subvoxels*. As depicted in Fig. 1, the grayscale templates had blurred edges because each pixel was the average of a set of pixels, simulating the aspect of metastases observed under MRI.

The next step was a 3D cross-correlation between the templates and the brain volume. Those pixels whose normalized cross-correlation coefficient (NCCC) exceeded a threshold of 75% of the maximum were established as pixels belonging to a BM. It was selected this 3D feature matching parameter because it is independent on the voxel intensity values. Its calculation was performed in the Fourier domain using a 3D extension of the Lewis's formula [9]. Although initially a detection consisted of several pixels, it was reduced to the pixel with highest NCCC.

It is noteworthy to understand that a 3D cross-correlation is not a slice by slice correlation and thus, the obtained detections are supposed to be located at the centroid of the 3D object. Despite this affirmation, employing a NCCC threshold of 75% caused that elongated structures were detected in several slices because for the algorithm they were a succession of ellipsoids. Detections could be true positives (TP) or false positives (FP), such as blood vessels.

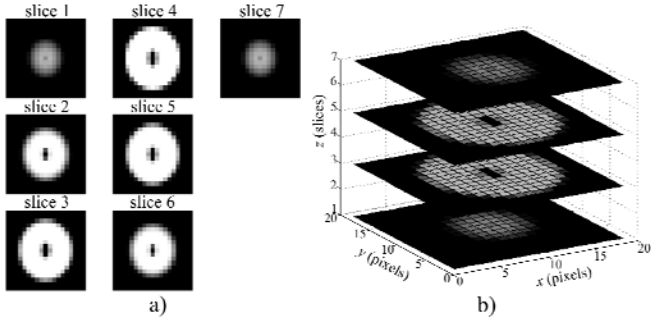

Figure 1. (a) Slices of an ellipsoidal tumor appearance template. (b) 3D template representation in gray colormap for visual purposes. The borders have a blurred aspect to mimic metastases observed in MRI.

C. Reduction of false positives

Firstly, to remove FP outside the patient's brain, the images were skull stripped using FSL-BET (FMRIB Centre, University of Oxford, Oxford, UK) [10]. It was a tough task due to anatomical deviation caused by brain metastases. Secondly, a segmentation-based method was applied in order to reduce FP inside the patient's brain.

The purpose was measuring the elongation of the object. Previously it was needed to segment the detections in the three orthogonal views by means of a level set [11], for template detected points to become contours. The selected region-based level set could detect objects whose edges were not necessarily defined by gradient, and energy was minimized using finite differences. The initial seed was a circle centered at the point detected by the templates, and the region of interest extended as the level set progressed.

First of all, the lesion candidates were segmented in axial, as the images were obtained in this view. Two criteria were required: an area up to 500 mm^2 and a major distance in *x* and *y* up to 50 mm. When this latter criteria were not accomplished, another region-based level set was employed [12] with less spreadable parameters. Final segmentation contained one single connected object. After each segmentation, the major distance in vertical or horizontal was calculated as the difference between the maximum and minimum coordinate in *x* or *y* axis. Subsequently, with the aim to separate metastases from blood vessels it was applied erosion followed by dilation to the contours whose ratio exceeded 3.

Axial segmentation was considered as gold truth. Hence, true segmentation in sagittal and coronal should not exceed more than 50% of respective axial measure and does not exceed 1500 mm^2. Otherwise, the segmentation was performed by the other level set [12] and as a last resort by an edge-based level set [13]. If any of the level sets met the criteria, the detection was not segmented. The same way as in axial, after each segmentation in sagittal and coronal, the major distance in vertical or horizontal was calculated. In Fig. 2a-c, a segmented metastasis is shown, depicting similar major distances. In contrast, in Fig. 2d-f a FP segmentation, sagittal sinus, shows different measures.

After segmentation, *distance_ratio* was calculated: ratio between maximum and minimum of major vertical or horizontal distance in each view, following (3). A threshold of 2.25 was selected in order to consider a metastatic slice: those objects whose ratio was less or equal to 2.25 were considered TP, and the rest were considered FP. Afterwards, the contours were stored in a binary matrix, and connected in 3D to find slices belonging to the same structure. To check if a slice was far or not from the threshold, all the slices whose ratio was between 2.25 and 2.25·1.3 were considered TP at the 3D structure.

$$distance\_ratio=\frac{max\left(major\ distance\ in\ each\ view\right)}{min\left(major\ distance\ in\ each\ view\right)} \quad (3)$$

In Fig. 2g, it is displayed in blue the slices whose ratio between distances was less or equal to 2.25 and thus

considered TP; in yellow, the FP changed to TP because their threshold was from 2.25 to 2.25·1.3 and colored in red the slices whose ratio overcame 2.25·1.3.

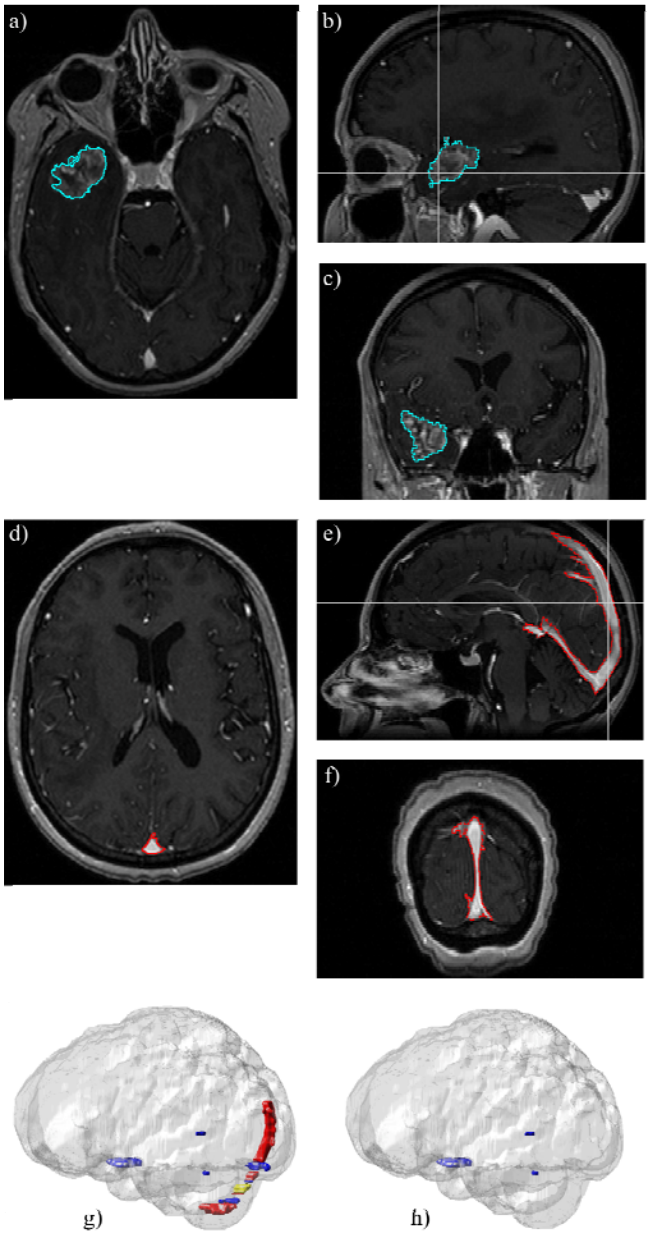

Figure 2. Metastasis segmentation in cyan: a) axial, b) sagittal and c) coronal. False positive segmentation in red: d) axial, e) sagittal and f) coronal. This segmentation allowed to calculate the ratio between maximum and minimum of the major vertical or horizontal distance in each view. g) Segmentations connected in 3D: blue, TP ratio up to threshold; yellow, TP ratio between threshold and threshold + 30%; red, FP ratio major than threshold + 30%. h) Remained lesion candidates.

All the slices of the 3D structure were turned to FP if the difference between considered TP slices and FP slices normalized by the number of slices was greater than one third of the number of slices (4) and the majority were FP slices (Fig. 2h). It was a conservative strategy that pretended to preserve the metastases.

$$\frac{|TPslices - FPslices|}{slices} \succ \frac{1}{3} slices \qquad (4)$$

III. RESULTS AND DISCUSSION

Template matching algorithm detected 58 of the 62 metastases, with a sensitivity of 93.55%. Features which allowed four lesions as false negatives (FN) were: excessive hypointensity at the center of the metastasis or sharp ring shape and small size (around 2.5 mm). The obtained FP rate per slice was 0.64 (Table I). This relatively high rate was mainly due to the superior sagittal sinus and its terminal branches are similar to metastases in both shape and intensity. The smallest template often detected choroid plexus, internal carotid arteries, basilar artery, internal cerebral veins and straight sinus. On the other hand, the other templates usually detected sagittal, straight, sphenoid, transverse and sigmoid sinus.

Regarding the method for FP reduction, Fig. 2a-c shows a metastatic slice segmentation whose ratio is 1.05, whereas Fig. 2d-f is a FP, the sagittal sinus, with a much higher ratio, 9.77. Blood vessels have a larger major ratio than BM and therefore, differentiating between FP and BM. Fig. 2h shows 3D connectivity algorithm results: there are 3 structures, 2 of them TP and 1 FP. The segmentation-based algorithm has lead to encouraging results: the FP rate per slice decreased to 0.15 and only one BM was removed (Table I).

TABLE I. OBTAINED RESULTS FOR NINETEEN PATIENT DATABASE

Method	**Measures**	
	Sensitivity	***False positive rate per slice***
Templates	93.55 %	0.64
False positive reduction	91.94 %	0.15

It is needed the three orthogonal views as, blood vessels such as the superior sagittal sinus are almost circular in axial slices, as depicted in Fig. 2d, leading a ratio between maximum distance in horizontal and vertical close to 1, classified as TP. Despite few metastases are attached to blood vessels in axial, they are also attached in the other two views and they are not removed because the ratio is lower than the threshold. Another advantage resides in major distance, calculated in horizontal or vertical as the difference between maximum and minimum coordinate in x or y axis. This way is simpler and faster than other degree of anisotropy calculations by means of an ellipse or ellipsoid.

As future lines, after applying an algorithm to delimit and segment each lesion, it is convenient to calculate more exactly how elongated the objects are. One reliable form is calculating the degree of anisotropy (DA) in 3D. The fastest method is the Ellipsoid of Inertia (EI) [14,15], a graphical representation of the tensor of inertia with respect to the center of mass. This geometrical shape allows to calculate DA as the ratio between its major and minor semiaxis. Fig. 3 shows the completely segmented BM and FP of Fig. 2, whose 3D DA is 1.5 (almost isotropic) and 8.5 (very anisotropic), respectively. Since the objects are not yet

segmented in all the slices, because they have been solely detected in some slices close to the centroid, it makes no sense to form a 3D structure. In that case, the minor axis would be considered the distance between these few slices and the 3D DA would be incorrect.

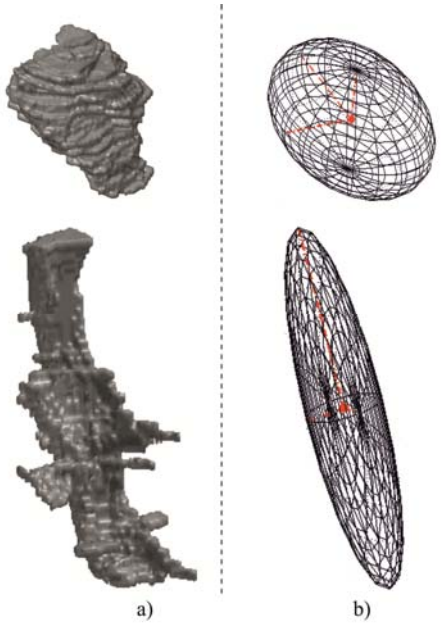

Figure 3. (a) 3D representation of a metastasis (above) and a false positive (below). (b) Corresponding Ellipsoid of Inertia with the inertia axes displayed in red.

Ambrosini et al. [2] applied their algorithm to 79 BM with a diameter from 3 to 45 mm (median = 7 mm), giving a sensitivity of 89.9% and a FP rate per image slice of 0.22. Brain segmentation was based on a 3D brain atlas that allowed to remove dural venous sinuses and internal carotid arteries, the major sources of FP. Our sensitivity is higher (91.94% vs 89.9%), with a lower FP rate per slice (0.15 vs 0.22). On the other hand, Nie et al. [3] employed a dataset containing 27 BM smaller than 8 mm in diameter. The experimental results showed a sensitivity of 81.5% and a FP rate per slice of 0.45. Other template-based method was developed by Farjam et al. [4] with promising results: a sensitivity of 93.5% and a FP rate of 0.024 with BM less than 5 mm in diameter. In our database, there are 30 metastases greater than 8 mm, so a direct comparison cannot be made with the last two methods. Current method is neither comparable with the symmetry-based methods [6,7] that worked well for medium and large metastases but not for small ones. The black-blood pulse sequence applied by Yang et al. [5] was beneficial. The authors obtained a sensitivity of 81.1% and a specificity of 98.2% in a database containing 53 BM smaller than 6 mm in diameter.

IV. Conclusion

An algorithm for the detection of metastases on brain MR imaging with lower false positives is presented. Metastases follow general patterns of three-dimensional morphology and signal intensity profiles in MRI and therefore can be detected by morphological and contrast 3D templates, using cross-correlation and NCCC in frequency domain as a quick and precise similarity measure.

Current results are encouraging as they present a high detection rate and a manageable number of false positives. Most of the false positives obtained were elongated structures as venous sinuses or internal carotid arteries. Thus, majority of false positives could be removed establishing a threshold for the ratio of their measures in the three planes, a fast approximation of the degree of anisotropy. Once the lesions will be segmented in all the slices, 3D degree of anisotropy in axial could be an ideal complement removing false positives.

This CAD tool serves as a support to the radiologic diagnosis by providing the analysis of hundreds of images.

References

[1] C. S. Platta, D. Khuntia, M. P. Mehta, and J. H. Suh, "Current treatment strategies for brain metastasis and complications from therapeutic techniques. A review of current literature," *Am. J. Clin. Oncol.*, vol.33, pp. 398-407, 2010.

[2] R. D. Ambrosini, P. Wang, and W. G. O'Dell, "Computer-aided detection of metastatic brain tumors using automated three-dimensional template matching," *J. Magn. Reson. Imaging*, vol. 31, pp. 85-93, 2010.

[3] S. -D. Nie, X. -S. Liu, X. -W. Sun, and Z. -X. Chen, "Computer-aided detection of brain metastases using MR images," *Chin. J. Biomed. Eng.*, vol. 29, pp. 677-682, 2010.

[4] R. Farjam, H. A. Parmar, D. C. Noll, C. I. Tsien, and Y. Cao, "An approach for computer-aided detection of brain metastases in post-Gd T1-W MRI," *Magnet. Reson. Med*., vol.30, pp. 824-836, 2012.

[5] S. Yang, Y. Nam, M. -O. Kim, E. Y. Kim, J. Park, and D. -H. Kim, "Computer-aided detection of metastatic brain tumors using magnetic resonance black-blood imaging," *Invest. Radiol.,* vol. 48, pp. 113-119, 2013.

[6] H. Khotanlou, O. Colliot, J. Atif, and I. Bloch, "3D brain tumor segmentation in MRI using fuzzy classification, symmetry analysis and spatially constrained deformable models," *Fuzzy Sets Syst.,* vol. 160, pp. 1457-1473, 2009.

[7] B. N. Saha, N. Ray, R. Greiner, A. Murtha, and H. Zhang, "Quick detection of brain tumors and edemas: A bounding box method using symmetry," *Comput. Med. Imaging Graph.,* vol. 36, pp. 95-107, 2012.

[8] P. Wang, A. DeNunzio, P. Okunieff, and W. G. O'Dell, "Lung metastases detection in CT images using 3D template matching," *Med. Phys*., vol. 34, pp. 915-922, 2007.

[9] J. P. Lewis, "Fast normalized cross-correlation," San Rafael, *CA: Industrial Light and Magic*, 1996.

[10] S. Smith, "Fast robust automated brain extraction," *Hum. Brain Mapp*., vol. 17, pp. 143-155, 2002.

[11] T. Dima, J. Domingo, and E. Dura, "A local level set method for liver segmentation in functional MRI imaging," *Nuclear Science Symposium and Medical Imaging Conference (NSS/MIC)*, *IEEE* pp. 3158-3161, 2011.

[12] T. Chan, and L. Vese, "Active contours without edges," *IEEE Trans. Image Process*., vol.10, pp. 266-277, 2001.

[13] V. Caselles, R. Kimmel, and G. Sapiro,"Geodesic active contours," *Int. J. Comput. Vis.,* vol. 22, pp. 61-79, 1997.

[14] F. P. Beer, E. R. Johnston, Jr, E. R. Eisenberg, W. E. Clausen, and G. H. Staab, *Vector mechanics for engineers, statics and dynamics,* 7th ed. New York: McGraw Hill. 2004, pp. 512–544.

[15] U. Pérez-Ramírez, J. J. López Orive, E. Arana, M. Salmerón-Sánchez, and D. Moratal, "Micro-computed tomography image-based evaluation of 3D anisotropy degree of polymer scaffolds," *Comput. Methods Biomech. Biomed. Engin.,* 2013 Aug 15. [Epub ahead of print] DOI:10.1080/10255842.2013.818663.